BIOCHEMISTRY
including biophysical chemistry & molecular biology
Article

Biochemistry **2009,** *48,* 11807–11816 11807
DOI: 10.1021/bi900920k

Preclusion of Irreversible Destruction of Dr Adhesin Structures by a High Activation Barrier for the Unfolding Stage of the Fimbrial DraE Subunit †

Rafał Piątek,*,‡,∥ Piotr Bruździak,§,∥ Beata Zalewska-Piątek,‡ Józef Kur,‡ and Janusz Stangret§

‡*Department of Microbiology and* §*Department of Physical Chemistry, Gdańsk University of Technology, ul. Narutowicza 11/12, 80-233 Gdańsk, Poland.* ∥*These authors contributed equally to this work.*

Received June 2, 2009; Revised Manuscript Received November 5, 2009

ABSTRACT: Dr fimbriae of uropathogenic *Eschericha coli* strains are an example of surface-located adhesive structures assembled via the chaperone−usher pathway. These structures are crucial for specific attachment of bacteria to host receptors. Dr fimbriae are linear associates of DraE proteins, the structure of which is determined by a donor strand complementation between the consecutive subunits. The biogenesis of these structures is dependent on a function of the specific periplasmic chaperone and outer membrane usher proteins. In a consequence of these structural and assembly properties the potential unfolding of a single subunit in a linear associate would cause a destruction of fimbrial adhesion function. This correlates with the observed high resistance of fimbrial structures for denaturation. In this paper we show that the mechanism of thermal denaturation of DraE-sc protein is well described by an irreversible two-state model which is the reduced form of a Lumry−Eyring protein denaturation model. In theory of this model the observed stability of DraE-sc protein is determined by the high activation barrier for the unfolding stage N → U. The microcalorimetry experiments permit to determine kinetic parameters of the DraE-sc unfolding process: energy of activation of 463.5 ± 20.8 kJ·mol^{-1} and rate constant of order 10^{-17} s^{-1}. This corresponds to the dissociation/unfolding half-life of Dr fimbriae of 10^8 years at 25 °C. The FT-IR experiments show that the high stability of DraE is determined by the cooperative rigid protein core. The presented mechanism of kinetic stability of Dr fimbriae is probably universal to adhesive structures of the chaperone−usher type.

The ability of microorganisms to specific adhesion to cellular host receptors is a crucial step in pathogenesis. Most Gram-negative bacteria possess specific secretion systems for the formation of complex adhesive organelles (*1*, *2*). The best known system is a chaperone−usher pathway identified in most pathogenic Gram-negative bacterial strains (*3*−*7*). The example of adhesive structures is Dr fimbriae encoded by a *dra* gene cluster of uropathogenic *Escherichia coli* strains causing pyelonephritis (*8*, *9*). Dr fimbriae are homopolymeric structures composed of DraE[1] fimbrial subunits with DraD protein incorporated at the tip of the fiber (*8*, *10*−*13*). The DraE fimbrial subunit is an adhesin which specifically binds to DAF glycoprotein and type IV collagen (*8*, *14*−*18*).

There are many available structural data which allow to define the molecular mechanism of bioassembly of adhesive organelles of chaperone−usher type (*4*, *19*−*24*). The structural subunits of adhesive systems are secreted into periplasmic space via the Sec pathway. The structural subunits have a conserved immunoglobulin-like fold lacking the C-terminal G β-strand. Therefore, the subunits possess a structure of a six-stranded β-sandwich with hydrophobic acceptor cleft formed by the edge strands. Specific periplasmic chaperone protects the subunits against nonspecific aggregation and enables them to fold into native conformation. The chaperone has a G1 donor β-strand which in complex with the subunit occupies the acceptor cleft (*4*, *25*−*27*). The binary chaperone−subunit complexes are targeted to the usher located in the outer membrane where the subunits are assembled into linear fibers. The mechanism is connected with releasing of subunits from the chaperone. In the course of a donor strand exchange reaction the N-terminal donor strand of incoming subunits replaced the donor strand of the chaperone from the acceptor cleft (*4*, *19*, *21*, *27*). So in the binary complex and in the linear fiber the subunits possess the acceptor cleft occupied by the donor strand. The structure of DraE/AfaE-III proteins (98% identity) and other experimental data prove that the mechanism of bioassembly of Dr fimbriae is in agreement with the model described above (*10*−*12*, *28*, *29*).

The process of formation of cellular adhesive structures follows without input of external source of energy. Structural and biochemical data concerning the biogenesis of *Yersinia pestis* F1 adhesin show that the energy required for this process is folding energy preserved by the chaperone at the stage of binary complex formation (*21*, *30*). Similar conclusions can be drawn based on structures of *E. coli* type P pili (*20*, *21*). The G1 β-strand of chaperone inserts deeply into the acceptor cleft of the subunits preventing a formation of the structured hydrophobic core by the residues of β-sheets. In the binary complex the subunit with

†This work was supported by the Ministry of Science and Higher Education, Grant 2218/B/PO1/2008/34.

*Corresponding author: tel, +48 58 347 24 17; fax, +48 58 347 24 17; e-mail: wejraf@o2.pl.

[1]Abbreviations: C_p^{ex}, excess heat capacity; DraE, adhesive subunit of Dr fimbriae; DraE-sc, self-complemented DraE subunit; DSC, differential scanning calorimetry; DTT, 1,4-dithiothreitol; FT-IR, Fourier transform infrared spectroscopy; OD_{600}, optical density of bacterial culture measured at 600 nm; PFA, principal factor analysis; T_m, protein melting temperature; k_{obs}, observed rate constant of protein unfolding; E_a, energy of activation of protein unfolding process; $\tau_{1/2}$, unfolding half-life of protein.

Published on Web 11/05/2009

expanded high energetic conformation possesses structure similar to molten globule. During the formation of linear fiber according to donor strand exchange reaction the subunit core collapses to condensed and energetically more stable conformation (*20*, *21*, *30*).

There is little information concerning the energetic aspects of formation and stability of adhesive structures (*30*−*33*). Zavialov et al. (*30*) published the thermodynamic data for formation of the binary Caf1−Caf1 M complex and minimal F1 fiber composed of two and three Caf1 subunits as well as self-complemented Caf1. Puorger et al. (*32*, *33*) determined the thermodynamic and kinetic parameters describing the stability of self-complemented FimH-sc and FimG-sc subunits of type 1 pili. The subunits are thermally denatured at temperatures above 80 °C with significant melting enthalpy of 600−800 kJ·mol^{-1}. In the case of FimH-sc and PapG-sc subunits the authors determined the unfolding kinetic rate constant of magnitude of 10^{-18} s^{-1}, corresponding to a half-life of 10^9 years at 25 °C. The data suggest that the subunits of adhesive structures possess a high thermodynamic and kinetic stability protecting them from denaturation.

The adhesive structures assembled via chaperone−usher pathway are enormously stable supramolecular protein associates that possess a high resistance to the thermal and chemical denaturation (*10*, *34*, *35*). In this paper we investigated the potential sources of this stability by defining the kinetic and thermodynamic parameters of a DraE-sc unfolding transition. Finally, using the Lumry−Eyring model of protein denaturation, we conclude that in the observed stability of fimbrial structures important is the high energetic barrier connected with the step of subunit unfolding.

EXPERIMENTAL PROCEDURES

Protein Expression, Purification, and Sample Preparation. DraE-sc (self-complemented) is a recombinant fusion protein composed of the following segments in N to C direction: the N-terminal signal peptide, the His_6 tag composed of six consecutive histidine residues connected by the single alanine residue with DraE, and the DraE β-sandwich lacking N-terminal donor strand GFTPSGTTGTTKLTVT and complemented at C-terminus by the same N-terminal donor strand using linker peptide DNKQ. The expression plasmid pET30-DraE-sc encoding DraE-sc was created by two consecutive PCR reactions and cloning. In the first step a native sequence of *draE* gene was amplified on a template of pBJN406 (encoding the whole *dra* gene cluster (*9*)) and cloned directionally into *Nde*I and *Hin*dIII restriction sites of the pET30b(+) vector (Novagen Merck Biosciences, Darmstadt, Germany) to generate the pET30-DraE recombinant plasmid. Then the *draE-sc* was amplified using the pBJN406 (as the template) and nucleotide primers: forward primer 5′-tatgagctccgcgcatgctcaccatcatcatcatcatgcgGAAGAGTGCCAGGTACGGGTTGGTGACCTGAC-3′ (*Sac*I site and the 3′ end of sequence encoded signal sequence is underlined, the sequence coding His Tag and linker alanine is in lower case, the complementary sequence is in upper case) and reverse primer 5′-tataagctttcaggtaacggtcagtttggtggtaccggtggtgccagacggggtgaaaccctgtttgttgtcTTTTGCCCAGTAACCCCCGGTCAGGGTCAG-3′ (the *Hin*dIII restriction site and stop codon are underlined, the sequence encoding linker peptide and donor strand is in lower case, the complementary sequence is in upper case). The obtained PCR product of *draE-sc* encodes the whole DraE-sc protein without the sequence of a signal peptide. The obtained PCR product was cloned into the pET30-DraE recombinant plasmid using *Sac*I and *Hin*dIII restriction sites. The *Sac*I site is located at 3′ end of the native *draE* sequence encoding the signal peptide. The DraE-sc protein was produced in *E. coli* BL21(DE3)/pET30-DraE-sc strain using the following procedure: 100 mL of an overnight culture was inoculated in 2 L of LB medium; the culture was grown with agitation at 37 °C to OD_{600} = 0.3, induced by adding IPTG to final concentration of 0.5 mM, and grown for an additional 2 h. The periplasmic fraction containing the mature DraE-sc protein was extracted from the harvested cells (*36*). The DraE-sc was purified by Ni^{2+}-affinity chromatography on IMAC Sepharose 6 Fast-Flow resin (GE Healthcare Bio-Sciences AB, Uppsala, Sweden) and eluted with a 5−500 mM imidazole gradient. The elution fraction was dialyzed against 20 mM phosphate buffer, pH 7.5, and 100 mM NaCl. The DraE-sc was finally purified by exclusion chromatography on a Superdex 75 10/300 GL column (Amersham Biosciences, Uppsala, Sweden) with 20 mM phosphate buffer, pH 7.5, and 100 mM NaCl. To microcalorimetry experiments the DraE-sc protein was concentrated by using an Amicon Ultra concentrator (Millipore, Bedford, MA) to a final concentration of ca. 1 mg·mL^{-1}. To the FT-IR analysis the DraE-sc was further dialyzed against 10 mM phosphate buffer, pH 7.5, and then 10 mL of protein sample with concentration of 1 mg mL^{-1} was lyophilized.

The Dr finbriae were purified as described previously and finally prepared to the FT-IR experiments as in the case of the DraE-sc (*37*).

Microcalorimetry. DSC experiments were performed on a CSC 6300 Nano-DSC III differential scanning microcalorimeter (Calorimetry Sciences Corp., Lindon, UT) with capillary cell volume of 0.299 mL in the temperature range from 15 to 100 °C. The experimental data were recorded using DSCRun software (Calorimetry Sciences Corp., Lindon, UT). The concentration of DraE-sc (molecular mass 16.32 kDa) was ca. 1 mg·mL^{-1} in each experiment. For the analysis of kinetic effects, we used different heating scan rates: 0.5, 1.0. 1.5, and 2.0 °C min^{-1}. Before each measurement, samples were degassed with stirring in an evacuated chamber for 10 min at room temperature and then carefully loaded into the cells. Calorimetric cells were kept under excess of 0.3 MPa to prevent degassing during the scan. The reversibility of the thermal transition was verified by checking the reproducibility of the calorimetric trace in second heating of the sample after cooling from the first scan and 30 min equilibration at low temperature. A dialysis buffer (20 mM phosphate, pH 7.5, 100 mM NaCl) was used in both cells to determine baselines that were subtracted from the sample runs to generate the DSC thermograms that were analyzed. To obtain the C_p^{ex}, the ORIGIN software package (MicroCal, GE Healthcare, U.K.) was used for a baseline subtraction and determination of total enthalpy change. The baseline correction of DSC curves was carried out using "chemical" baseline, referring to the fraction of unfolded (U) state of protein. Fitting of the theoretical equation to the experimental heat capacity profiles was carried out using a program written by us in the Matlab 6.5 (MathWorks, Inc., Natick, MA) environment.

FT-IR Spectroscopy. About 3 mg of lyophilized mixture of protein and phosphate buffer was dissolved in D_2O (final concentration of protein ca. 20 mg·mL^{-1}) 24 h before the experiment to allow all accessible hydrogen atoms to exchange to deuterium. In the case of samples containing reducing agent, lyophilized protein was similarly dissolved in 10 mM solution of DTT in D_2O.

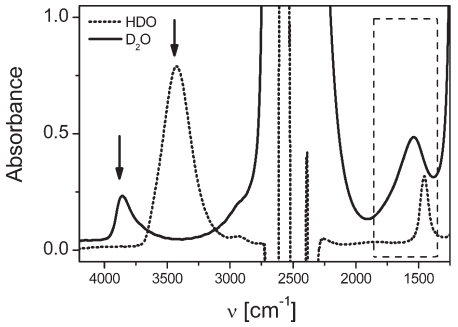

FIGURE 1: Isolated FT-IR spectra of HDO and D_2O. Isolated spectra of HDO (dotted line) and D_2O (solid line). Arrows indicate bands used to control process of subtraction of these spectra from spectrum of protein. Dashed rectangle indicates the region of spectra particularly important for the analysis of protein spectra.

All spectra were measured in a Nicolet 8700 spectrometer (Thermo Electron Scientific Inc., Waltham, MA) using an electrically heated transmission cell (Harrick Scientific Products Inc., Pleasantville, NY) with CaF_2 windows and 56 μm Teflon spacers. The spectrometer was purged with dry nitrogen to diminish water vapor influence. Spectra were averaged using 64 or 32 scans for lower and higher temperatures, respectively. OMNIC (Thermo Fisher Scientific Inc., Waltham, MA) and Grams/32 (Galactic Ind. Corp., Salem, MA) softwares were used to collect and analyze spectra.

The direct calculation of second derivative of measured spectra, without solvent subtraction, allows to obtain information about the composition of the amide I′ band. The band shape of D_2O in this spectral region is nearly a flat line, and its share in second derivative is negligible (*38*). This method does not require solvent (D_2O) subtraction from the measured raw transmission spectra. The direct usage of second derivatives allow to get reliable information about amide I′ composition even in a situation of the low protein concentration. The Savitzky–Golay's algorithm has been used to calculate all second derivatives, using 13 cm^{-1} width and third-order polynomial (*39*).

The shape of the residual amide II during hydrogen–deuterium exchange precludes the usage of second derivatives to analyze its quantity and composition. The valuable method of obtaining information about its behavior is to subtract spectra of pure D_2O and the proper amount of isolated HDO formed during H/D exchange of H_2O bonded on the surface of lyophilized protein and from the H/D exchange of protein amide protons. The best possible indicators of appropriate spectra subtraction, as was found in our laboratory, are two relatively weak bands near 3850 and 3300 cm^{-1} for D_2O and HDO, respectively (Figure 1). To obtain isolated spectra of HDO, appropriate for described method, two temperature series of spectra have to be measured: possibly purest D_2O and D_2O with a small additive of H_2O (short incubation in open air is sufficient). After subtraction of two spectra at appropriate temperature, isolated spectrum of HDO in this temperature is obtained. It is also necessary to obtain pure spectrum of D_2O in similar manner as described above. One could also in the first place subtract measured spectrum of D_2O, without HDO correction, and next subtract appropriate amount of isolated HDO spectrum.

To reduce undesirable effects of baseline drift and other interferences, a chemometric technique has been used: principal factor analysis (PFA). Spectra reproduction is possible, assuming that there is a limited number of principal factors (PF) responsible for protein part of spectra and other factors corresponding to undesirables features of spectra. PFA was performed in Matlab 6.5 (MathWorks, Inc., Natick, MA) using the factor analysis toolbox (Applied Chemometrics Inc., Sharon, MA).

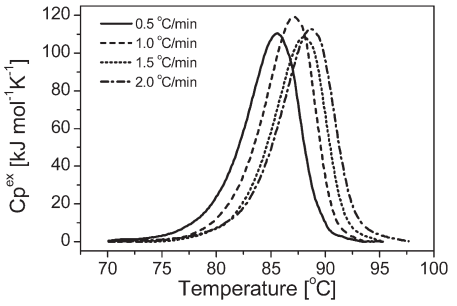

FIGURE 2: DSC thermograms of DraE-sc at different scanning rates. Experimental dependencies of excess heat capacity (C_p^{ex}) on temperature for DraE-sc protein, obtained at different scanning rates.

RESULTS

Convergence of the Mechanism of DraE-sc Denaturation with Kinetic Two-State Irreversible Model. To investigate the thermal stability and the mechanism of thermal denaturation of the DraE-sc a series of DSC experiments, with scanning rates of 0.5, 1.0, 1.5, and 2.0 °C min^{-1}, have been conducted. The DSC thermograms (Figure 2) clearly show that the denaturation profile is scan-rate dependent. Maximum of DSC peaks shifts approximately linearly toward higher temperatures together with an increase of scanning rate. The mean temperature of the DraE-sc melting, T_m, was determined on a level of 87.35 °C with minimal 85.6 °C and maximal 88.7 °C value for scanning rates 0.5 and 2.0 °C min^{-1}, respectively. In the reheating scan small endothermic peak with area corresponding to ca. 5% (depending on scan rate) of the first peak was observed. In the next reheating scans no visible endothermic effects were detected indicating that the transition process was irreversible (data not shown). Strong relationship between the scanning rate and the temperature of the transition maximum indicates that the denaturation of DraE-sc is a kinetically controlled process. This excludes the usage of a simple two-state equilibrium model. This kind of denaturation process is assumed to be a first-order reaction with a rate constant that changes with temperature, according to Arrhenius equation. To analyze such DSC data, the simplest kinetic two-state reduced form of the Lumry–Eyring model was applied (*40*):

$$\mathrm{N} \xrightarrow{k_{obs}} \mathrm{F} \tag{1}$$

where N denotes native state of protein, F stands for denatured irreversible state, and k_{obs} is the observed rate constant. The rate of transition between these states is limited by the energy of activation, which is determined by the conformation of the transition state. The nonlinear least-squares curve-fitting procedure of experimental DSC data to eq 2 was applied (Figure 3):

$$C_p^{ex} = \frac{1}{v}\Delta H \exp\left[\frac{E_a}{R}\left(\frac{1}{T^*} - \frac{1}{T}\right)\right] \exp\left\{-\frac{1}{v}\int_{T_0}^{T} \exp\left[\frac{E_a}{R}\left(\frac{1}{T^*} - \frac{1}{T}\right)\right] dT\right\} \tag{2}$$

where C_p^{ex} is the excess heat capacity, v is the temperature scanning rate, ΔH is the denaturation enthalpy (assumed to be constant in the temperature range of transition), E_a is energy of

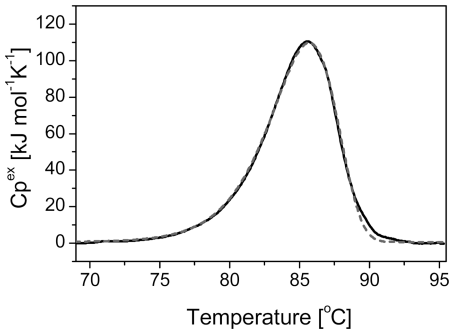

FIGURE 3: Curve fitting of DraE-sc DSC thermogram. The thermogram of DraE-sc protein obtained at a scanning rate of 0.5 °C min^{-1} and the result of fitting of experimental excess heat capacity curve, after baseline subtraction, to the two-state kinetic model of protein unfolding (eq 2): (solid line) experimental curve; (dashed line) fitted curve.

activation, R is gas constant, and T^* is temperature (at absolute scale) at which $k = 1$ min^{-1} (*41*). The obtained χ^2 test values (ca. 1 or below) show that applied model describes experimental data very well. Although fitted curve described experimental data quite well, additional tests were employed to confirm the legitimacy of usage of the two-state irreversible model of protein unfolding. According to Kurganov et al. (*40*) the following anamorphoses of experimental DSC curves were used: dependency of ln C_p^{ex} on the reciprocal value of temperature (Figure 4A), dependency of reciprocal value of temperature on $\ln[\nu C_p^{ex}/(Q_t - Q)]$ (Figure 4B), and dependency of $(1 - Q/Q_t)^\nu$ on temperature (Figure 4C), where Q_t is the total heat absorbed during transition (calorimetric enthalpy) and Q is the heat absorbed during heating of protein from reference temperature T_0 (starting point of transition) to the temperature T. In the case of each test the obtained curves share common shape. This suggests that the two-state irreversible model describes the thermal transition of the DraE-sc sufficiently.

The E_a and T^* values, two parameters characterizing irreversible thermal transition of proteins, estimated by fitting eq 2 to experimental data of different scanning rates are quite similar. Simultaneously, the obtained values of transition parameters (ΔH, E_a, T^*, k, and $\tau_{1/2}$) are presented in Table 1. The mean value of the activation energy, E_a, was calculated as 463.5 ± 20.8 kJ·mol^{-1}, and the mean value of temperature T^* was determined as 89.25 ± 0.32 °C. The estimation of energy of activation based on extrapolation of straight lines in Figure 3 gives coincident results. T^* values might be considered as scan-rate independent and do not change together with temperature of transition. The obtained values of T^* for different experiments are in a very good agreement, varying with only 0.4% of calculated T^* mean value. Discrepancy between values of activation energy E_a is relatively small and equals 4.5% of mean value.

The presented calorimetric data show that the thermal denaturation of DraE-sc is a kinetically controlled process well described by one transition two-state unfolding reduced form of Lumry−Eyring model. The DraE-sc is a very stable protein with the mean melting temperature of 87.35 °C and corresponding transition enthalpy of 712.5 ± 45.9 kJ·mol^{-1}. The stability of DraE-sc is demonstrated by kinetic parameters: rate constant and energy of activation. The obtained rate constant of unfolding process of magnitude 10^{-17} s^{-1} corresponds to calculated enormously high value of half-life time at 25 °C of the order of

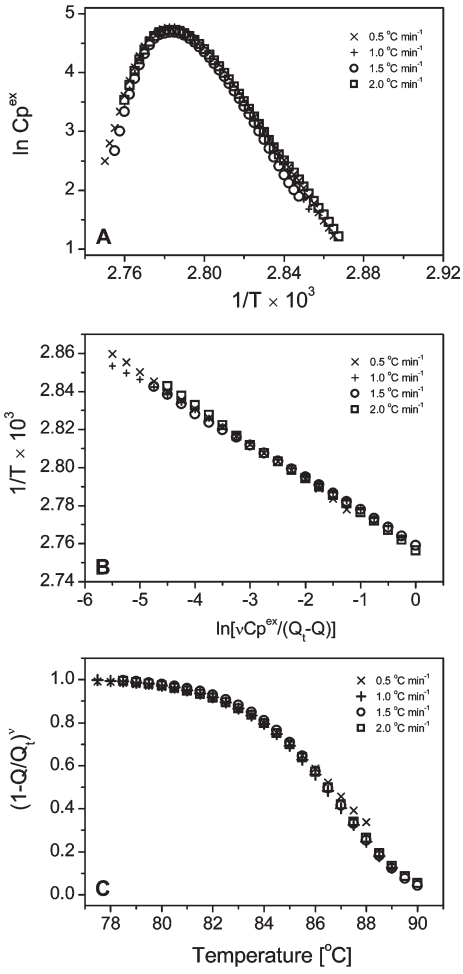

FIGURE 4: Anamorphoses of DSC thermograms of DraE-sc. Three graphical anamorphoses of experimental temperature dependencies of excess heat capacity C_p^{ex} at different scanning rates. (A) Dependency of ln C_p^{ex} on the reciprocal value of temperature (in absolute scale). (B) Dependency of reciprocal value of temperature (in absolute scale) on $\ln[\nu C_p^{ex}/(Q_t - Q)]$. (C) Dependency of $(1 - Q/Q_t)^\nu$ on temperature.

10^8 years. This value coincides well with the parameters determined for FimG and FimH proteins complemented with the specific donor strand (*33*).

DraE-sc Subunit as an Appropriate Minimal Model of Dr Fimbriae: FT-IR Study. Fourier transform infrared spectroscopy (FT-IR) is a powerful technique, widely used to study the secondary structure of proteins. The main band most often used to analyze the FT-IR data is so-called the amide I′, corresponding almost entirely to the C═O stretching vibrations of polypeptide backbone (1600−1700 cm^{-1}). Due to structural constraints the vibration frequencies of individual secondary structures are slightly different, making it possible to determine the structural composition of particular protein (*42*−*44*).

The FT-IR spectra of DraE-sc are characterized by the amide I′ band with maximum at 1636 cm^{-1} which points out that the main structural component of protein is β-sheet (Figure 5A). The analysis of fitted component bands of the amide I′ band (Figure 5A) shows that β-sheet structures with maximum at 1634 and 1683 cm^{-1} take up ca. 62% of the whole amide I′ area. The occurrence of minor band at 1683 cm^{-1} might denote that the observed β-sheet is composed of antiparallel strands. The turns and short loops (ca. 1659 cm^{-1}) take up ca. 30% of the amide I′ area and together with β-sheets are main structural

Table 1: Thermodynamic and Kinetic Parameters of DraE-sc Unfolding[a]

scan rate (°C min^{-1})	ΔH (kJ·mol^{-1})	$E_a{}^1$ (kJ·mol^{-1})	$E_a{}^2$ (kJ·mol^{-1})	T^* (°C)	k_{obs} (s^{-1})	$\tau_{1/2}$ (years)
0.5	706	449	439	89.5	1.68×10^{-16}	131.2×10^6
1.0	741	475	485	89.1	3.12×10^{-17}	704.6×10^6
1.5	675	474	483	89.1	3.30×10^{-17}	666.2×10^6
2.0	728	456	444	89.3	1.14×10^{-16}	193.1×10^6
mean	712.5 ± 45.9	463.5 ± 20.8	462.8 ± 39.2	89.25 ± 0.32		

[a]Thermodynamic and kinetic parameters of DraE-sc unfolding obtained by fitting the two-state kinetic model of DSC transition (eq 2) to experimental thermograms. ΔH, enthalpy of unfolding; $E_a{}^1$, energy of activation obtained by fitting eq 2; $E_a{}^2$, energy of activation obtained by extrapolation of fitted graph from Figure 3; T^*, temperature at which $k = 1$ min^{-1}; k_{obs}, observed rate constant of protein unfolding at 25 °C; $\tau_{1/2}$, unfolding half-life at 25 °C. k_{obs} and $\tau_{1/2}$ were determined from the parameters of fitted eq 2.

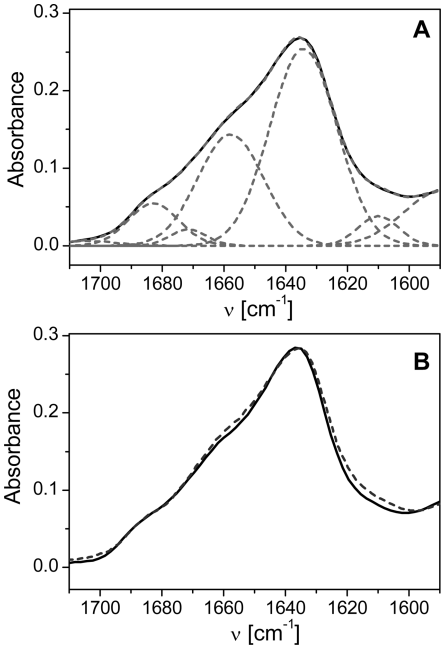

FIGURE 5: Analysis of the amide I′ band of DraE-sc and its comparison with Dr fimbriae. (A) The result of curve-fitting procedure of DraE-sc spectrum in temperature of 30 °C (solid line). Component bands (dashed line) approximated with Gauss peak function. Fitted curve (sum of component bands) presented as dashed line. (B) Comparison of DraE-dsc FT-IR spectrum (solid line) and Dr fimbriae spectrum (dashed line).

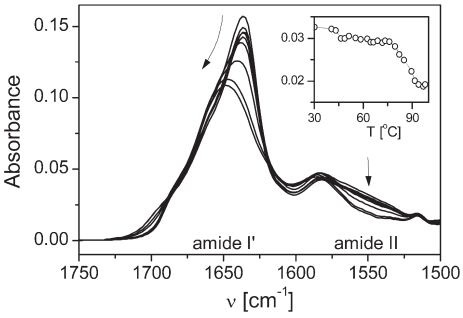

FIGURE 6: PFA reproduced temperature series of DraE-sc spectra. The PFA reproduced amide I′ and amide II bands of FT-IR spectra of DraE-sc protein in temperature range of 30.4−98.0 °C. The spectra measured in transmission mode using D_2O as solvent. Arrows indicate directions of major changes in band positions and intensities with increasing temperature. Inset: Intensity of amide II band in function of temperature.

components of the DraE-sc protein. These spectral data well correlate with the known structures of DraE/AfaE-III proteins and their homologues (*12*, *28*).

The FT-IR spectrum of the isolated native Dr fimbriae has been measured and compared with appropriate DraE-sc spectrum. As can be seen from Figure 5B both spectra are very similar in shape. The maxima of both amide I′ bands are the same (ca. 1636 cm^{-1}). The only differences are visible in the region of turn structures (ca. 1660 cm^{-1}) and low wavenumber bands (ca. 1618 cm^{-1}) and might indicate some kind of little differences in the structure. This alteration probably concerns the regions of contact between two adjacent subunits. These data clearly show that the DraE-sc might be considered as the minimal structural model of native Dr fimbriae. Similar approach exploiting the self-complemented subunits was used to specify the stability of F1 antigen of *Y. pestis* and type 1 pili of *E. coli* (*30*, *33*). Puorger et al. (*33*) showed that the FimG-sc protein in which a donor strand was covalently attached to the C-terminus of protein possesses lower stability than the FimG with noncovalently attached donor peptide. The authors suggest that these phenomena may be connected with the steric consternation exerted by linker sequence that connected the donor strand. So we conclude that the data presented in this publication characterizing the stability of DraE-sc may differ a little from the stability of DraE subunits in native Dr fimbriae adhesin.

Extraordinary Stability of DraE-sc Secondary Structure in High Temperatures. To investigate the dynamics and the character of DraE-sc unfolding, the FT-IR experiment concerning heating of a liquid solution of the protein was performed. The series of FT-IR transmission spectra of DraE-sc in D_2O as a solvent corresponding to an increase of temperature was presented in Figure 6. The temperature ranged from 30.4 to 98.0 °C. An increase of temperature up to ca. 75 °C does not affect the shape of amide I′ band significantly. However, small changes (increase of absorption) are visible in the loop region (1640−1650 cm^{-1}) and ca. 1670 cm^{-1} which might be assigned to the increased thermal mobility of these structures and probably the side chains of amino acid residues. The observed slight decrease of a band intensity might be attributed to the thermal expansion of the liquid sample inside the cell.

The spectrum of unfolded protein (Figure 6) contains a strong and broad main peak, with maximum near 1650 cm^{-1}. This corresponds to unfolded disordered structures and long loops (*45*, *46*). The shape of the amide I′ band during decreasing of temperature does not change (data not shown), indicating that the protein does not recover its native structure. These observations indicate that the mechanism of denaturation of the DraE-sc protein in conditions of the FT-IR experiment performed is irreversible.

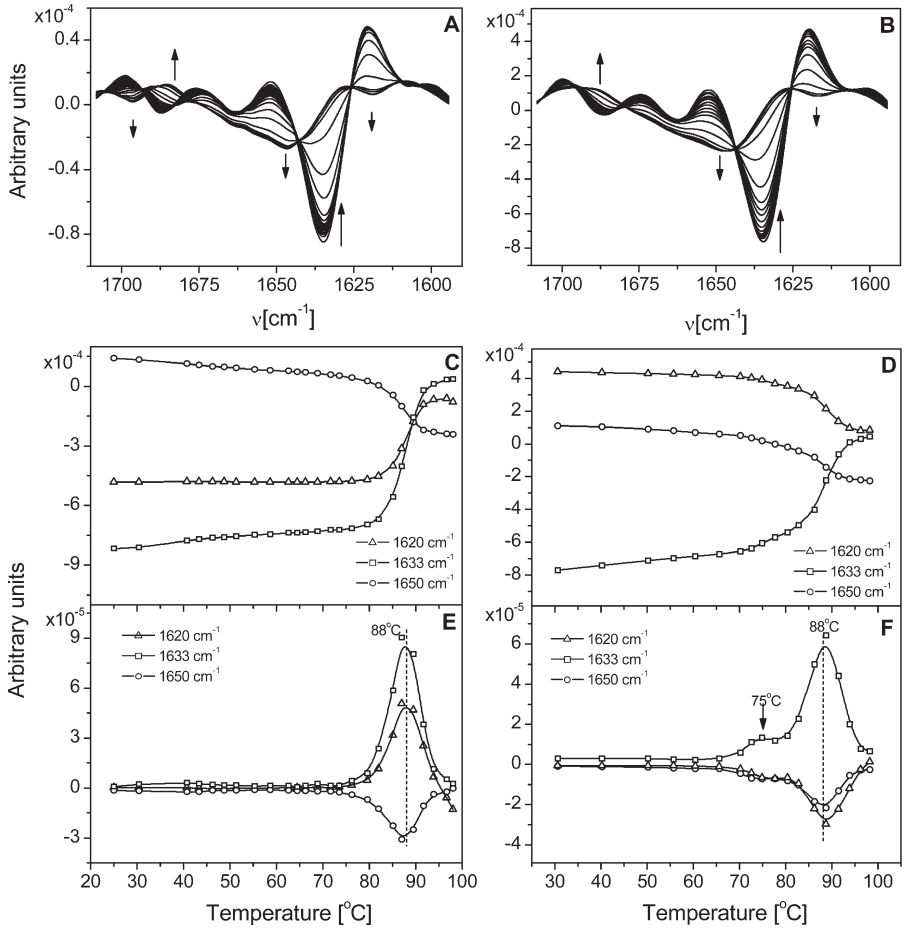

FIGURE 7: Second derivative spectra and transition curves of DraE-sc. (A) Second derivatives of FT-IR spectra of DraE-dsc (the amide I′ band) in temperature range of 25.4−98.0 °C and (B) second derivatives of FT-IR spectra of DraE-dsc (the amide I′ band) in the presence of 10 mM DTT in temperature range of 30.6−98.2 °C. Arrows indicate changes in curve shape with increasing temperature. (C, D) Transition curves determined on the basis of second derivatives of DraE-dsc (C) and DraE-dsc in the presence of 10 mM DTT (D) for 1620, 1633, and 1650 cm^{-1}, respectively. (E, F) Derivatives of transition curves from panels C and D with marked temperatures of transitions.

The calculated second derivatives of the analyzed spectra are presented in Figure 7A. The slight decrease of the second derivative intensity might be assigned to concentration decrease due to thermal expansion of the sample inside cell, similar effect to that mentioned before. The structural features of DraE-sc obtained from the analysis of the second derivatives are consistent with the results of curve-fitting procedure. Similarly, main component band of the second derivatives is characteristic to β-sheets (1635 cm^{-1}), and a small component band near 1686 cm^{-1} confirms this observation. The other band near 1663 cm^{-1} corresponds to short loops and β-turns. The second derivative of denatured DraE in high temperature is quite characteristic to typical denatured protein structure. A weak band near 1618 cm^{-1} might be assigned to absorption of amino acid side chains, probably tyrosine or another aromatic amino acid residue (C−C stretching, C−H in-plane bending). The broad peak with maximum ca. 1642 cm^{-1} corresponds to long loops or unordered polypeptide. It seems to retain some residual structure because of its "rough" shape. Possibly, other weak component bands are present, dominated by main component band. Thus it can be carefully stated that the DraE-sc retains residual structure in high temperatures, probably due to the presence of disulfide bond.

The temperature profiles, created by graphing a dependency of absorbance on temperature, indicate that there is only one transition of protein structure with midpoint temperature of 88 °C. No other transitions are visible indicating that the transition is a simple cooperative process. These profiles were drawn independently for three wavenumbers, 1620, 1650, and 1633 cm^{-1}, corresponding to various secondary structures. The midpoints of transitions were determined by differentiating transition curves (Figure 7E). A maximum of arising peak indicated the temperature of protein "melting". A large coincidence of behavior of these three different structures suggests that this transition is strictly cooperative.

Similar transition curves have been drawn for Dr fimbriae spectral series to investigate a similarity of denaturation temperatures of the DraE-sc and DraE homopolymer (Figure 8). The obtained temperature is very similar; thus it may be stated that denaturation of these polymeric structures corresponds to denaturation of the subunit.

The PF analysis of the series of DraE-sc FT-IR spectra suggests that there are only three significant factors responsible for the observed changes during heating of protein liquid sample. But only two of them can be assigned to changeability of amide I′ band shape, because the third factor does not have any influence in this spectral region and might be omitted in further analysis. Using algorithm developed by Malinowski et al. the approximate spectra of pure factors might be isolated (*47*). Spectra of these factors are presented in Figure 9. We want to stress that these spectra are very similar to the spectra of native and unfolded forms of the examined protein. Even shape of weak amide II (ca. 1550 cm^{-1}) is reproduced quite well. As expected, loadings of

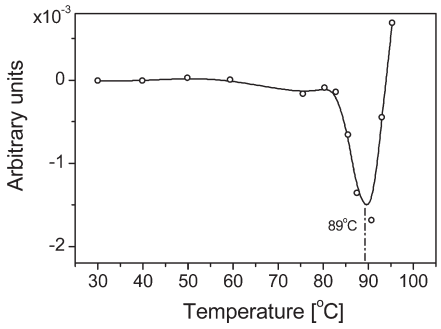

FIGURE 8: Determination of melting temperature of Dr fimbriae. Derivative of transition curve determined on the basis of intensity of second derivative band at 1619 cm^{-1} of Dr fimbriae spectral series. Dashed line indicates transition temperature.

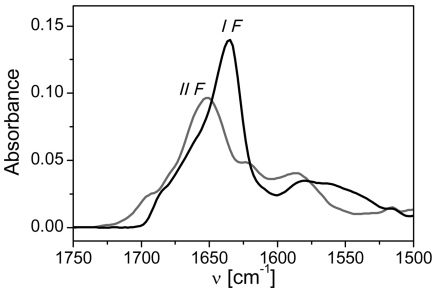

FIGURE 9: Isolated spectra of principal factors of the DraE-sc spectra series. Isolated spectra of the first (corresponding to native protein) and second (corresponding to denatured protein) principal factor (PF), based on the principal factor analysis of DraE-sc protein spectral series using three principal factors. The third principal factor (not shown) represents fluctuations of baseline and possibly other disturbances introduced during D_2O/HDO subtraction.

these two factors coincide very well with the obtained transition curves, indicating that no other transition species are presented and no other transition occurs in the observed temperature range.

Confirmation of High Stability of the DraE-sc Core by H/D Exchange. The use of D_2O as a solvent allows to observe changes of the so-called amide II band that corresponds mainly to N−H bending vibrations. The extent to which proteins exchange hydrogens to deuterium can be monitored with the intensity of the residual amide II band (ca. 1550 cm^{-1}) during heating experiments. Long enough incubation of lyophilized protein in D_2O causes that the most of hydrogen atoms engaged in formation of secondary structures are exchanged to heavier isotope. In the case of rigid and highly packed proteins solvent molecules do not have free access into the core of protein; thus some of the protons have no possibility to exchange. Though the amide II′ is located near 1450 cm^{-1}, in mentioned situation a part of the amide II is still visible near 1550 cm^{-1}. This kind of resistance is often observed in the case of membrane proteins, where even after 72 h of incubation in D_2O up to 70% of hydrogen atoms are retained (*48*). Small soluble proteins act differently; i.e., most of the hydrogen atoms are exchanged quite quickly, in time scale of second or minutes, but often the residual amide II is visible. This amide II band might act in two ways during heating. In the case of mentioned before membrane proteins the exchange is accomplished often during denaturation. It can also disappear in temperature below the temperature of denaturation, indicating that the structure of protein is quite weak and prone to solvent penetration even before denaturation, e.g., myoglobin (*49*), RNase H, or HEW lysozyme (*50*).

During 24 h incubation of lyophilized DraE-sc protein in D_2O at 25 °C the most of hydrogen atoms engaged in formation of secondary structures are exchanged to heavier isotope. However, there is a clearly visible residual amide II band, corresponding to nonexchanged protons (Figure 6). The small size of residual amide II might be easily understood when one realizes that DraE-sc protein is quite small (150 residues) and almost all H atoms engaged into the formation of secondary structures are located on the surface layer of the protein. Thus, observed exchange resistance of some protons confirms rigidity of DraE-sc protein with regard to globular proteins with similar molecular weight. To analyze the rigidity of DraE-sc, we follow the exchange of observed residual protons to deuterium during heating of protein sample at temperature range from 25.4 to 98.0 °C. The intensity of amide II does not change visibly in spectral series in temperature range from 25 to 75 °C. The hydrogen−deuterium exchange of residual hydrogen atoms of DraE-sc begins and is accomplished only during transition of protein from native to denatured state. The temperature profile obtained at 1550 cm^{-1} (inset in Figure 6) coincides quite well with transition curves obtained for changes in the intensity of second derivative bands.

Thus the observed mechanism of proton exchange classifies the stability of DraE-sc between membrane and small globular proteins. These analyses clearly show that the observed high melting temperature of the DraE-sc coincides well with protein rigidity demonstrated by temperature-induced proton exchange experiments.

Effective Reduction of DraE-sc by DTT Occurs at the Stage of Protein Unfolding Transition. To analyze the rigidity of structure of DraE-sc, we performed experiment in which we observed the influence of reducing agent 1,4-dithiothreitol (DTT) on thermal denaturation of protein. Generally, in the case of small globular proteins stabilized by the disulfide bonds an addition of reducing agent to denaturation experiments highly decreases temperature of melting. This process is dependent on the access of DTT to disulfide bond that usually in proteins is buried in core and excluded from solvent. In the case of globular proteins with highly cooperative hydrophobic core we may suspect that the influence of reducing agent on denaturation transition will be limited. The DraE-sc protein possesses one disulfide bond that connects adjacent strands in the vicinity of the acceptor cleft. In the structure of DraE protein the disulfide bond is almost totally excluded from the solvent. The series of FT-IR spectra of DraE-sc in the presence of 10 mM DTT have been measured in temperature range from 30.6 to 98.2 °C. The conditions of the sample were selected to make the reduction of disulfide bonds possible. The structural characteristic of DraE-sc up to the beginning of thermal unfolding transition in the presence of reducing agent is the same as previously described, and no changes in secondary structure are visible. Second derivative spectra with corresponding temperature profiles and their derivatives are presented in Figure 7B,D,F. In the temperature range of unfolding transition the main difference between this and previous series is lack of one component band near 1696 cm^{-1} appearing during denaturation of the DraE-sc protein in nonreducing environment. The second-derivative spectrum of denatured protein seems to be smoother than the corresponding spectrum of protein in nonreducing conditions, even though all operations performed at both series of spectra were the same. This might indicate that the reduction of the disulfide bond during protein unfolding causes complete loss of secondary structure. On the contrary to the previous series, two overlapping

transitions with midpoints at 75 and 88 °C were visible in the temperature range of protein unfolding (Figure 7F). The main transition with midpoint at 88 °C is identical to that observed in the case of DraE-sc in the presence of no reducing agent. The much smaller pretransition with midpoint at 75 °C is unique to unfolding performed in the presence of 10 mM DTT. The source of this transition at this stage is not well recognized. Despite this, most of the protein denatures at 88 °C, indicating that DTT does not have possibility to effectively reduce disulfide bond until the protein loses the compactness connected with the main unfolding transition. All spectroscopic FT-IR data presented in this paper connect the observed high thermal stability of DraE-sc with rigidity of the highly cooperative protein core.

DISCUSSION

Adhesive organelles assembled via the chaperone−usher pathway possess structure based on the complementation of Ig-like fold by N-terminal donor strand of consecutive subunits. The secretion system is based on the activity of chaperone located in the periplasm and outer membrane usher proteins that perform the donor strand complementation and the donor strand exchange reactions (*7*, *13*). In consequence, a potential denaturation of fimbrial subunits at the cell surface is irreversible and causes a destruction of adhesive organelles crucial for surviving of cells. The temperature of denaturation of DraE-sc determined calorimetrically and spectrally is the same as the melting temperature of Dr fimbriae adhesin. This confirms the model in which thermal denaturation of Dr adhesin is a natural consequence of destruction of DraE subunits.

To explain the sources of high stability of Dr fimbrial structures, we analyzed calorimetric measured process of thermally induced DraE-sc unfolding in the context of the Lumry−Eyring model of protein denaturation. This model is described by general eq 3:

$$N \leftrightarrow U \rightarrow F \quad (3)$$

where N denotes the native states, U is the unfolded state, and F represents the final state which results from the irreversible alteration of the U state (*41*). In this model, the irreversible protein denaturation is thought to have at least two steps: (a) reversible unfolding of native protein and (b) irreversible alteration of the unfolded protein to the final state which is unable to fold back to the native state. In living cells the proteins, especially their unfolded states, are exposed to many irreversible alterations (aggregation, proteolysis). In such a situation, if the irreversible alterations of U state are characterized by the high rate constant in the temperature range of denaturation process, the Lumry−Eyring model can be reduced to the one-step irreversible model N → F (eq 1 used to characterize the DraE-sc denaturation) (*41*). In this case denaturation process is phenomenologically described by the two-state model in which only the native and final states are significantly populated and the conversion from N to F is determined by strongly temperature-dependent, observed first-order rate constant k_{obs}. The presented Lumry−Eyring model suggests that the native state is relatively safe and that, for the protein to become susceptible to irreversible alterations, it must cross the activation barrier for unfolding (*51*). So the best possible mechanism of preventing the irreversible denaturation of fimbrial subunits and in consequence destruction of fimbriae adhesin is low rate constant for the unfolding step N → U.

To verify this mechanism, we performed the calorimetric and spectroscopic FT-IR experiments that characterize the stability parameters of DraE-sc, the minimal Dr fimbriae model. In the calorimetric DSC experiments the DraE-sc protein denatures in accordance to the kinetic two-state (one-step) irreversible model N → F. This mechanism is supported by spectral FT-IR analysis. The process of denaturation is characterized by high temperature of melting (T_m = 88 °C) and transition enthalpy of value 712.5 ± 45.9 kJ·mol^{-1}. The application DSC method and Lumry−Eyring model for analysis of calorimetric data give the energy of activation E_a = 463.5 ± 20.8 kJ·mol^{-1} and rate constant of unfolding k_{obs} of order 10^{-17} s^{-1} for the process at 25 °C. This calculated rate constant corresponds to a half-life of unfolding of 10^8 years. Obtained data clearly show that the kinetic stability based on high energy of activation and low rate constant for denaturation stage N → U is crucial to determine the resistance of Dr adhesin against irreversible inactivation. The calorimetric data coincide with the spectral FT-IR analysis in qualitative description of dynamics of secondary structure change during process of thermal denaturation. The DraE-sc protein spectra are unchanged until the moment in which the process of cooperative denaturation undergoes. The high stability of the DraE-sc is confirmed by the facts that the full exchange of residual protons and reduction of the disulfide bond buried in the hydrophobic core followed by FT-IR occur only at the stage of denaturation.

The presented thermodynamic and kinetic data are related to values obtained for denaturation process of Caf1-sc, FimH-sc, and FimG-sc proteins (*30*, *33*). The mentioned proteins denature at temperature above 80 °C with high enthalpy of transition within range of 600−800 kJ·mol^{-1}. In the case of FimH-sc and FimG-sc the rate constant and corresponding half-life of unfolding are available and prove very high kinetic stability of these proteins. The results presented in this work and previously published characterize the stability of three adhesive structures with different morphology: Caf1, amorphous F1 antigen of *Y. pestis*; FimH and FimG, type 1 pili of *E. coli*; DraE, Dr fimbriae of *E. coli*. Additionally, F1 anitgen and Dr fimbriae belong to FGL chaperone-assembled fimbrial homopolymeric polyadhesins, and type 1 pili are FGS chaperone-assembled heteropolymeric adhesive structures (*13*, *25*). It permits to suggest that the high kinetic stability is characteristic to all chaperone−usher adhesive structures from Gram-negative bacteria.

ACKNOWLEDGMENT

The calorimetric measurements were made at the laboratory of the Center of Excellence ChemBioFarm at Gdansk University of Technology, equipped due to the grant from the European Regional Development Funds.

REFERENCES

1. Jonson, A. B., Normark, S., and Rhen, M. (2005) Fimbriae, pili, flagella and bacterial virulence. *Contrib. Microbiol. 12*, 67–89.
2. Le Bouguénec, C. (2005) Adhesins and invasins of pathogenic *Escherichia coli*. *Int. J. Med. Microbiol. 295*, 471–478.
3. Hung, D. L., and Hultgren, S. J. (1998) Pilus biogenesis via the chaperone/usher pathway: an integration of structure and function. *J. Struct. Biol. 124*, 201–220.
4. Sauer, F. G., Futterer, K., Pinkner, J. S., Dodson, K. W., Hultgren, S. J., and Waksman, G. (1999) Structural basis of chaperone function and pilus biogenesis. *Science 285*, 1058–1061.
5. Sauer, F. G., Barnhart, M., Choudhury, D., Knight, S. D., Waksman, G., and Hultgren, S. J. (2000) Chaperone-assisted pilus assembly and bacterial attachment. *Curr. Opin. Struct. Biol. 10*, 548–556.

6. Vetsch, M., Erilov, D., Molière, N., Nishiyama, M., Ignatov, O., and Glockshuber, R. (2006) Mechanism of fibre assembly through the chaperone-usher pathway. *EMBO Rep. 7*, 734–738.
7. Remaut, H., Tang, C., Henderson, N. S., Pinkner, J. S., Wang, T., Hultgren, S. J., Thanassi, D. G., Waksman, G., and Li, H. (2008) Fiber formation across the bacterial outer membrane by the chaperone/usher pathway. *Cell 133*, 640–652.
8. Swanson, T. N., Bilge, S. S., Nowicki, B., and Moseley, S. L. (1991) Molecular structure of the Dr adhesin: nucleotide sequence and mapping of receptor-binding domain by use of fusion constructs. *Infect. Immun. 59*, 261–268.
9. Nowicki, B., Barrish, J. P., Korhonen, T., Hull, R. A., and Hull, S. I. (1987) Molecular cloning of the *Escherichia coli* O75X adhesin. *Infect. Immun. 55*, 3168–3173.
10. Piatek, R., Zalewska, B., Kolaj, O., M., F., Nowicki, B., and Kur, J. (2005) Molecular aspects of biogenesis of *Escherichia coli* Dr Fimbriae: characterization of DraB-DraE complexes. *Infect. Immun. 73*, 135–145.
11. Cota, E., Jones, C., Simpson, P., Altroff, H., Anderson, K. L., du Merle, L., Guignot, J., Servin, A., Le Bouguénec, C., Mardon, H., and S., M. (2006) The solution structure of the invasive tip complex from Afa/Dr fibrils. *Mol. Microbiol. 62*, 356–366.
12. Anderson, K. L., Billington, J., Pettigrew, D., Cota, E., Simpson, P., Roversi, P., Chen, H. A., Urvil, P., du Merle, L., Barlow, P. N., Medof, M. E., Smith, R. A., Nowicki, B., Le Bouguénec, C., Lea, S. M., and Matthews, S. (2004) An atomic resolution model for assembly, architecture, and function of the Dr adhesins. *Mol. Cell 15*, 647–657.
13. Zavialov, A., Zav'yalova, G., Korpela, T., and Zav'yalov, V. (2007) FGL chaperone-assembled fimbrial polyadhesins: anti-immune armament of Gram-negative bacterial pathogens. *FEMS Microbiol Rev. 31*, 478–514.
14. Nowicki, B., Moulds, J., Hull, R., and Hull, S. (1988) A hemagglutinin of uropathogenic *Escherichia coli* recognizes the Dr blood group antigen. *Infect. Immun. 56*, 1057–1060.
15. Pham, T., Kaul, A., Hart, A., Goluszko, P., Moulds, J., Nowicki, S., Lublin, D. M., and Nowicki, B. J. (1995) dra-related X adhesins of gestational pyelonephritis-associated *Escherichia coli* recognize SCR-3 and SCR-4 domains of recombinant decay-accelerating factor. *Infect. Immun. 63*, 1663–1668.
16. Selvarangan, R., Goluszko, P., Singhal, J., Carnoy, C., Moseley, S., Hudson, B., Nowicki, S., and Nowicki, B. (2004) Interaction of Dr adhesin with collagen type IV is a critical step in *Escherichia coli* renal persistence. *Infect. Immun. 72*, 4827–4835.
17. Servin, A. L. (2005) Pathogenesis of Afa/Dr diffusely adhering *Escherichia coli*. *Int. J. Med. Microbiol. 295*, 471–478.
18. Korotkova, N., Yarova-Yarovaya, Y., Tchesnokova, V., Yazvenko, N., Carl, M. A., Stapleton, A. E., and Moseley, S. L. (2008) *Escherichia coli* DraE adhesin-associated bacterial internalization by epithelial cells is promoted independently by decay-accelerating factor and carcinoembryonic antigen-related cell adhesion molecule binding and does not require the DraD invasin. *Infect. Immun. 76*, 3869–3880.
19. Choudhury, D., Thompson, A., Stojanoff, V., Langermann, S., Pinkner, J., Hultgren, S. J., and Knight, S. D. (1999) X-ray structure of the FimC-FimH chaperone-adhesin complex from uropathogenic *Escherichia coli*. *Science 285*, 1061–1066.
20. Sauer, F. G., Pinkner, J. S., Waksman, G., and Hultgren, S. J. (2002) Chaperone priming of pilus subunits facilitates a topological transition that drives fiber formation. *Cell 111*, 543–551.
21. Zavialov, A. V., Berglund, J., Pudney, A. F., Fooks, L. J., Ibrahim, T. M., MacIntyre, S., and Knight, S. D. (2003) Structure and biogenesis of the capsular F1 antigen from *Yersinia pestis*: preserved folding energy drives fiber formation. *Cell 113*, 587–596.
22. Korotkova, N., Le Trong, I., Samudrala, R., Korotkov, K., Van Loy, C. P., Bui, A. L., Moseley, S. L., and Stenkamp, R. E. (2006) Crystal structure and mutational analysis of the DaaE adhesin of *Escherichia coli*. *J. Biol. Chem. 281*, 22367–22377.
23. Verger, D., Bullitt, E., Hultgren, S. J., and Waksman, G. (2007) Crystal structure of the P pilus rod subunit PapA. *PLoS Pathog. 3*, 73.
24. Gossert, A. D., Bettendorff, P., Puorger, C., Vetsch, M., Herrmann, T., Glockshuber, R., and Wüthrich, K. (2008) NMR structure of the *Escherichia coli* type 1 pilus subunit FimF and its interactions with other pilus subunits. *J. Mol. Biol. 375*, 752–763.
25. Hung, D. L., Knight, S. D., Woods, R. M., Pinkner, J. S., and Hultgren, S. J. (1996) Molecular basis of two subfamilies of immunoglobulin-like chaperones. *EMBO J. 15*, 3792–3805.
26. Barnhart, M. M., Pinkner, J. S., Soto, G. E., Sauer, F. G., Langermann, S., Waksman, G., Frieden, C., and Hultgren, S. J. (2000) PapD-like chaperones provide the missing information for folding of pilin proteins. *Proc. Natl. Acad. Sci. U.S.A. 97*, 7709–7714.
27. Zavialov, A. V., Kersley, J., Korpela, T., Zav'yalov, V. P., MacIntyre, S., and Knight, S. D. (2002) Donor strand complementation mechanism in the biogenesis of non-pilus systems. *Mol. Microbiol. 45*, 983–995.
28. Pettigrew, D., Anderson, K. L., Billington, J., Cota, E., Simpson, P., Urvil, P., Rabuzin, F., Roversi, P., Nowicki, B., du Merle, L., Le Bouguénec, C., Matthews, S., and Lea, S. M. (2004) High resolution studies of the Afa/Dr adhesin DraE and its interaction with chloramphenicol. *J. Biol. Chem. 279*, 46851–46867.
29. Jedrzejczak, R., Dauter, Z., Dauter, M., Piatek, R., Zalewska, B., Mróz, M., Bury, K., Nowicki, B., and Kur, J. (2006) Structure of DraD invasin from uropathogenic *Escherichia coli*: a dimer with swapped beta-tails. *Acta Crystallogr., Sect. D: Biol. Crystallogr. 62*, 157–164.
30. Zavialov, A. V., Tischenko, V. M., Fooks, L. J., Brandsdal, B. O., Aqvist, J., Zav'yalov, V. P., Macintyre, S., and Knight, S. D. (2005) Resolving the energy paradox of chaperone/usher-mediated fibre assembly. *Biochem. J. 389*, 685–694.
31. Vetsch, M., Sebbel, P., and Glockshuber, R. (2002) Chaperone-independent folding of type 1 pilus domains. *J. Mol. Biol. 322*, 827–840.
32. Erilov, D., Puorger, C., and Glockshuber, R. (2007) Quantitative analysis of nonequilibrium, denaturant-dependent protein folding transitions. *J. Am. Chem. Soc. 129*, 8938–8939.
33. Puorger, C., Eidam, O., Capitani, G., Erilov, D., Grütter, M. G., and Glockshuber, R. (2008) Infinite kinetic stability against dissociation of supramolecular protein complexes through donor strand complementation. *Structure 16*, 631–642.
34. Eshdat, Y., Silverblatt, F. J., and Sharon, N. (1981) Dissociation and reassembly of *Escherichia coli* type 1 pili. *J. Bacteriol. 148*, 308–314.
35. Orndorff, P. E., and Falkow, S. (1984) Organization and expression of genes responsible for type 1 piliation in *Escherichia coli*. *J. Bacteriol. 159*, 736–744.
36. Zav'yalov, V. P., Chernovskaya, T. V., Chapman, D. A., Karlyshev, A. V., MacIntyre, S., Zavialov, A. V., Vasiliev, A. M., Denesyuk, A. I., Zav'yalova, G. A., Dudich, I. V., Korpela, T., and Abramov, V. M. (1997) Influence of the conserved disulphide bond, exposed to the putative binding pocket, on the structure and function of the immunoglobulin-like molecular chaperone Caf1M of *Yersinia pestis*. *Biochem. J. 324*, 571–578.
37. Zalewska, B., Piatek, R., Konopa, G., Nowicki, B., Nowicki, S., and Kur, J. (2003) Chimeric Dr fimbriae with a herpes simplex virus type 1 epitope as a model for a recombinant vaccine. *Infect. Immun. 71*, 5505–5513.
38. Mark, H., and Workman, J., Jr. (2007) Chemometrics in spectroscopy, Academic Press, New York.
39. Savitzky, A., and Golay, M. J. E. (1964) Smoothing and differentiation of data by simplified least squares procedures. *Anal. Chem. 36*, 1627–1639.
40. Kurganov, B. I., Lyubarev, A. E., Sanchez-Ruiz, J. M., and Shnyrov, V. L. (1997) Analysis of differential scanning calorimetry data for proteins. Criteria of validity of one-step mechanism of irreversible protein denaturation. *Biophys. Chem. 69*, 125–135.
41. Sanchez-Ruiz, J. M. (1992) Theoretical analysis of Lumry-Eyring models in differential scanning calorimetry. *Biophys. J. 61*, 921–935.
42. Arrondo, J. L. R., Muga, A., Castresana, J., and Goni, F. M. (1993) Quantitative studies of the structure of proteins in solution by Fourier-transform infrared spectroscopy. *Prog. Biochem. Mol. Biol. 59*, 23–56.
43. Arrondo, J. L. R., and Goni, F. M. (1999) Structure and dynamics of membrane proteins as studied by infrared spectroscopy. *Prog. Biochem. Mol. Biol. 72*, 367–405.
44. Barth, A., and Zscherp, C. (2002) What vibrations tell us about proteins. *Q. Rev. Biophys. 35*, 369–430.
45. Herberhold, H., Royer, C. A., and Winter, R. (2004) Effects of chaotropic and kosmotropic cosolvents on the pressure-iduced unfolding and denaturation of proteins: an FT-IR study on staphylococcal nuclease. *Biochemistry 43*, 3336–3345.
46. Weert, M. v. d., Haris, P. I., Hannink, W. E., and Crommelin, D. J. A. (2001) Fourier transform infrared spectrometric analysis of protein conformation: effect of sampling method and stress factors. *Anal. Biochem. 297*, 160–169.
47. Malinowski, E. R., Cox, R. A., and Haldna, U. L. (1984) Factor analysis for isolation of the Raman spectra of aqueous sulfuric acid components. *Anal. Chem. 56*, 778–781.

48. Sturgis, J., Robert, B., and Goormaghtigh, E. (1998) Transmembrane helix stability: the effect of helix-helix interactions studied by Fourier transform infrared spectroscopy. *Biophys. J. 74*, 988–994.
49. Meersman, F., Smeller, L., and Heremans, K. (2002) Comparative Fourier transform Infrared spectroscopy study of cold-, pressure-, and heat-induced unfolding and aggregation of myoglobin. *Biophys. J. 82*, 2635–2644.
50. Meersman, F., and Heremans, K. (2003) Temperature-induced dissociation of protein aggregates: accessing the denatured state. *Biochemistry 42*, 14234–14241.
51. Plaza del Pino, I. M., Ibarra-Molero, B., and Sanchez-Ruiz, J. M. (2000) Lower kinetic limit to protein thermal stability: a proposal regarding protein stability in vivo and its relation with misfolding diseases. *Proteins 40*, 58–70.